J. Fluid Mech. (1993), *vol.* 257, *pp.* 533–558

Elementary topology of two-dimensional turbulence from a Lagrangian viewpoint and single-particle dispersion

By DALILA ELHMAÏDI, ANTONELLO PROVENZALE† AND ARMANDO BABIANO

Laboratoire de Météorologie Dynamique, CNRS, Ecole Normale Superieure, Paris Cedex 05, France

(Received 25 May 1992 and in revised form 22 June 1993)

We discuss a series of numerical experiments on the dispersion of neutrally buoyant particles in two-dimensional turbulent flows. The topology of two-dimensional turbulence is parametrized in terms of the relative dominance of deformation or rotation; this leads to a segmentation of the turbulent field into hyperbolic and elliptic domains. We show that some of the characteristic structural domains of two-dimensional turbulent flows, namely coherent structures and circulation cells, generate particle traps and peculiar accelerations which induce several complex properties of the particle dispersion processes at intermediate times. In general, passive particles are progressively pushed from the coherent structures and tend to concentrate in highly hyperbolic regions in the proximity of the isolines of zero vorticity. For large dispersion times, the background turbulent field is a privileged domain of particle richness; there is however a permanent particle exchange between the background field and the energetic circulation cells which surround the coherent structures. At intermediate times, an anomalous dispersion regime may appear, depending upon the relative weight of the different topological domains active in two-dimensional turbulence. The use of appropriate conditional averages allows the basic topology of two-dimensional turbulence to be characterized from a Lagrangian point of view. In particular, an intermediate $t^{\frac{5}{4}}$ anomalous dispersion law is shown to be associated with the action of hyperbolic regions where deformation dominates rotation; the motion of the advected particles in strongly elliptic regions where rotation dominates over deformation is shown to be associated with a $t^{\frac{5}{3}}$ dispersion law. Because neutral particles concentrate on average in hyperbolic regions, the $t^{\frac{5}{4}}$ dispersion law is quite robust and it can be observed under very general circumstances.

1. Introduction

High vorticity concentrations inside coherent structures play a fundamental role in the dynamics of two-dimensional turbulence. Far from being homogeneously distributed, the vorticity field of two-dimensional flows is concentrated in localized domains behaving as coherent entities. These long-lasting vortices have lifetimes which greatly exceed the characteristic timescale of nonlinear turbulent interactions; in two-dimensional turbulence, coherent structures are much more stable than in three dimensions as vorticity can act only orthogonal to the flow. The existence of coherent structures induce a basic inhomogeneity of the velocity field. As a whole, two-

† Permanent address: Istituto di Cosmogeofisica del CNR, Corso Fiume 4, Torino, Italy.

dimensional turbulence can be considered as the synoptic result of a complex distortion process of the velocity field, caused and maintained by the carrying power of the coherent structures and by their interactions (McWilliams 1984, 1990; Benzi *et al.* 1986; Benzi, Patarnello & Santangelo 1987, 1988; Babiano *et al.* 1987*a*; Legras, Santangelo & Benzi 1988).

The above considerations indicate that two-dimensional turbulent fields are characterized by a complex topology in physical space. The characterization of this topology and the basic distinction between coherent structures and the surrounding turbulent field has been developed mainly in an Eulerian framework (McWilliams 1984; Brachet *et al.* 1988; Ohkitani 1991). The effects of coherent structures on the turbulent dispersion capacity and, more generally, their signatures in a Lagrangian framework are much less studied. However, the majority of experimental measurements of large-scale (almost two-dimensional) geophysical flows are in the form of Lagrangian observations of freely drifting buoys or free ballon tracking. In the present study, we consider the statistical effects of the coherent structures and, more generally, of the two-dimensional turbulence topology on the motion of Lagrangian tracers, in order to provide a starting point for the proper interpretation of the available experimental results.

The particle dispersion processes are herein studied by following the trajectories of an ensemble of neutral particles which are passively advected by a turbulent Eulerian velocity field; the latter has been obtained by numerically integrating the equations of two-dimensional turbulence. These Lagrangian techniques have been developed in the study of atmosphere and ocean dynamics; such methods allow an estimation of the space–time dynamical features of the flow and for identication of the basic non-homogeneous and non-isotropic mechanisms active in two-dimensional turbulence. In this context, two-dimensional turbulence arises from the interplay between an ensemble of high vorticity concentrations (coherent structures) and the surrounding background field characterized by low vorticity levels. Single particle trajectories are seen to develop, with different properties, in the various structural domains of two-dimensional turbulence.

A basic issue addressed in this study is to understand whether the different domains of two-dimensional turbulence may be associated with different particle dispersion properties. In general, single particle trajectories test different components of the turbulent field, owing to the particle moving among the various topological domains. In order to separate the different contributions, we show that a partitioning of the turbulent field into elliptic and hyperbolic domains provides an appropriate parametrization of the turbulence (Weiss 1981). The use of appropriate conditional averages on the set of advected particles then allows the different contributions to be distinguished. The results of this type of analysis indicate the existence of two intermediate anomalous dispersion regimes which may be unambiguously linked with the topology of two-dimensional turbulence. The problem of parametrizing the long-time dispersion coefficient as a function of topology will be addressed in a forthcoming paper.

The work reported in this paper has been motivated by the desire to understand the dynamics of Lagrangian tracers in geophysical flows. Clearly, real geophysical flows are much more complicated than pure two-dimensional turbulence. In particular, with rotating spherical geometry, Rossby waves drastically alter the dispersion properties, both directly (Bartello & Holloway 1991) and through their inhibition of the formation of coherent vortices (McWilliams 1984). Analogously, three-dimensionality may generate new effects not accounted for by two-dimensional turbulent flows. Two-

dimensional turbulent dynamics represent, however, a good approximation of these geophysical situations where the contributions of quasi-two-dimensional vortices is significant. In the present work we take the point of view that two-dimensional turbulence is one of the simplest systems where the richness of GFD flows is potentially encountered.

2. Elementary topology of two-dimensional turbulence

2.1. *Basic definitions*

A two-dimensional turbulent field may be decomposed in a simplified way by distinguishing the respective contributions of rotation and deformation to the square of the velocity gradient, i.e. by writing

$$\|\nabla \boldsymbol{U}\|^2 = \tfrac{1}{2}(\omega^2 + s^2), \tag{1}$$

where $\boldsymbol{U}$ is the Eulerian velocity field, ω refers to the vorticity and s to the deformation:

$$\omega = \partial_x v - \partial_y u, \quad s^2 = s_1^2 + s_2^2, \quad s_1 = \partial_x u - \partial_y v, \quad s_2 = \partial_x v + \partial_y u.$$

A more sophisticated decomposition has been proposed by Weiss (1981); this has been adopted for example by McWilliams (1984), Brachet *et al.* (1988) and Ohkitani (1991). If the strain rate along a particle path is slowly varying with respect to the vorticity gradient, the Lagrangian evolution of $\nabla\omega$ is then given by a linear differential equation whose solution is

$$\nabla\omega \approx \exp(\pm\tfrac{1}{2}Q^{\frac{1}{2}}t); \tag{2}$$

where

$$Q = s^2 - \omega^2. \tag{3}$$

Even though the Weiss approximation is rather crude, it has the advantage of simplifying the picture of two-dimensional turbulence by an elementary partitioning of the field into two distinct domains, namely (*a*) elliptic domains ($Q < 0$), where rotation dominates deformation, $\omega^2 > s^2$; and (*b*) hyperbolic domains ($Q > 0$), where deformation dominates rotation, $\omega^2 < s^2$. It is important to recall, however, that the elliptic domains may be associated either with the vortex cores or with those regions in the background turbulent sea among the coherent structures where the fluctuating Q-field takes negative values. Analogously, hyperbolic regions may be found either in the background turbulence or in the organized structures surrounding the vortex cores, which constitute what we call here the circulation cells. Strictly speaking, the dynamical importance of the two types of elliptic or hyperbolic regions may be quite different (e.g. coherent versus random evolution).

2.2. *Topology from Eulerian numerical simulations*

The barotropic two-dimensional vorticity equation has been integrated on a doubly periodic square lattice $(0, 2\pi; 0, 2\pi)$ by using a pseudo-spectral approximation (Basdevant *et al.* 1981). Dissipation of enstrophy near the cutoff scale is parametrized by the 'Iterated Laplacian Method'; a linear friction dissipates energy at larger scales. The details of the numerical simulations used in this work have been thoroughly described by Babiano *et al.* (1987*a*, 1990). The resolution of the Eulerian numerical simulations considered here is 128×128 and 512×512. The forcing is defined by keeping the amplitude of the zonal mode $(0, k_I)$ fixed. The type of forcing and dissipation chosen here have been widely employed in past numerical experiments. In the 128×128 experiment (called **R128F10**) we have chosen $k_I = 10$, the non-

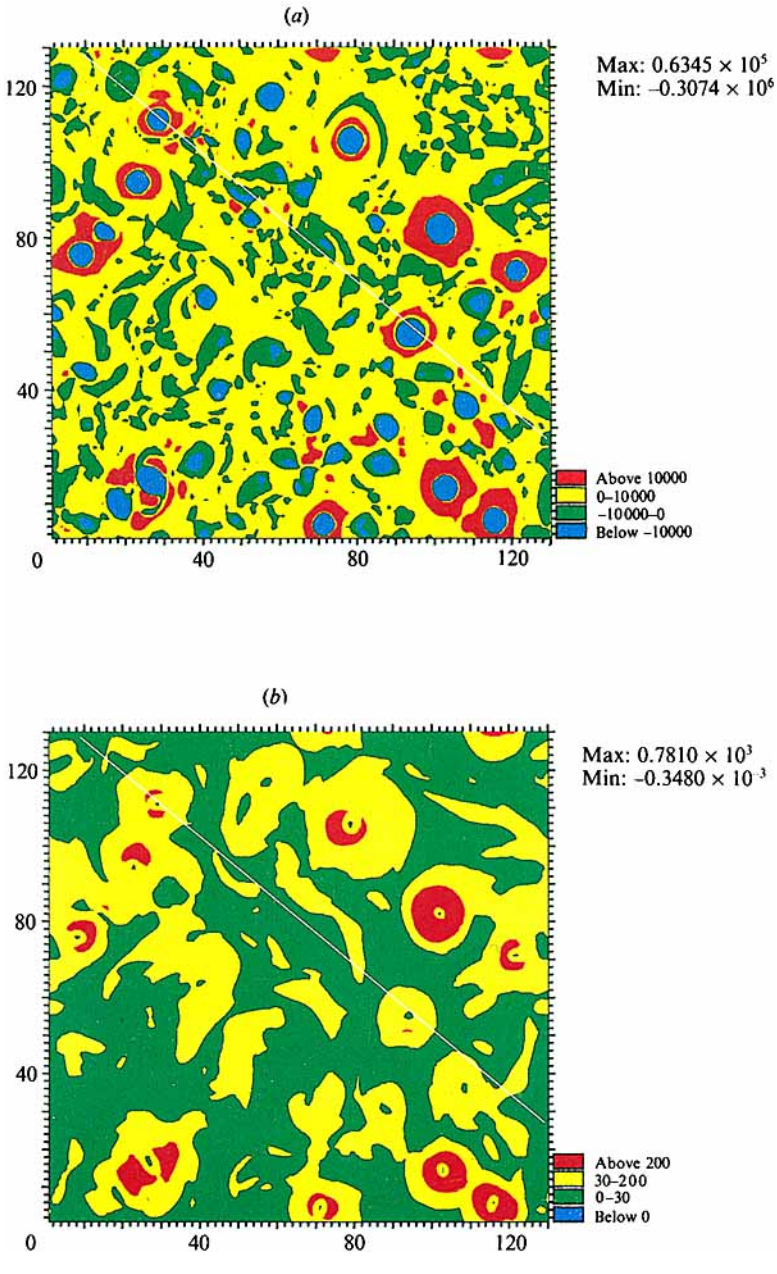

FIGURE 1. The spatial distribution of (*a*) $Q(x, y, t)$ and (*b*) the Eulerian kinetic energy $E(x, y, t)$ for the R128F10 numerical simulation of forced and dissipated, stationary two-dimensional turbulence. The different colours correspond to different values of Q and E, as indicated in each panel. The white line in each panel indicates where the cross-sections of the fields shown in figure 2 have been taken.

dimensional Eulerian kinetic energy of the field is $\bar{E} = 53.5$ and the non-dimensional Eulerian enstrophy is $\bar{Z} = 2600$. The mean non-dimensional Eulerian integral timescale is $\overline{T_E} = 0.14$, the mean non-dimensional Lagrangian integral timescale is $\overline{T_L} = 0.035$ and the time step is $\Delta t = 0.0001$. The scale factors used to non-dimensionalize the

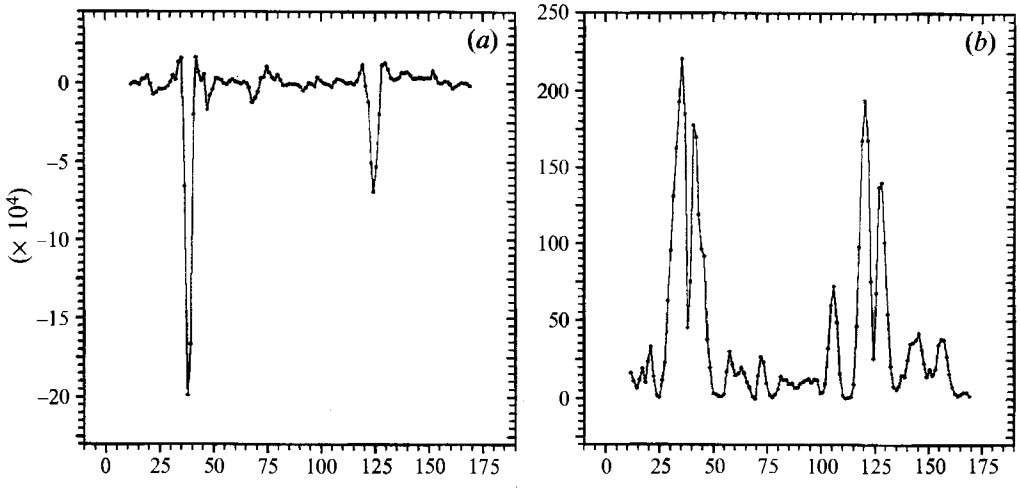

FIGURE 2. Cross-sections of (*a*) the Q and (*b*) the E fields shown in figure 1. The two cross-sections have been taken along the white lines cutting the fields in figure 1.

equations have been obtained by prescribing the forcing scale to be 50 km and the mean kinetic energy to be 12.5 $cm^2\ s^{-2}$. These constraints give the scale factors $t^+ = 330$ days and $l^+ = 159$ km. In the 512×512 experiment (called R512F40), we have chosen $k_I = 40$; in this case, the non-dimensional scale of the coherent structures is about four times smaller than for experiment R128F10. The non-dimensional Eulerian kinetic energy of simulation R512F40 is $\bar{E} = 627$ and the non-dimensional Eulerian enstrophy is $\bar{Z} = 126500$. The mean non-dimensional Lagrangian integral timescale is $\overline{T_L} = 0.013$; the time step is $\Delta t = 0.000025$ and the scale factors are $t^+ = 1304.6$ days and $l^+ = 636.6$ km. The present simulations represent a non-divergent two-dimensional approximation of the ocean dynamics without the β-effect.

The Lagrangian motions in the above Eulerian fields have been obtained by a particle advection scheme with a third-order spline interpolation and a second-order time integration. The feasibility of Lagrangian numerical experiments by integrating the particle motions in a numerically integrated Eulerian velocity field has been examined by Haidvogel (1982), Zouari & Babiano (1990) and by Zouari (1991).

A typical example of the structure of two-dimensional turbulence is given in figure 1(*a*, *b*), which shows respectively the spatial distribution of the quantity $Q(x, y, t)$ and of the Eulerian kinetic energy $E(x, y, t)$ as obtained from the R128F10 experiment. The corresponding vorticity field is given in figure 4. Figure 2(*a*, *b*) shows the cross-sections of Q and of the Eulerian turbulent energy E along a line encompassing the entire simulation domain (the cross-section is shown as a white line on the fields of figure 1*a*, *b*). In this type of turbulent flow, insulated coherent structures have approximately the same scale $D_I = \pi/k_I$, where k_I is the forcing mode. The inverse energy range is spectrally located between D_I and $D_E = \pi/k_E$, where k_E is the most energetic mode. In the present experiment, $k_I = 10$ and $k_E = 3.3$. The scales D_I and D_E are respectively of 6.4 and 19.4 grid intervals. The particular value of the forcing scale considered here provides a limited number of well-defined vortices with well-developed circulation cells, as it can be seen from figure 1(*a*, *b*).

A partitioning based on the Weiss criterion would divide the turbulent field only into elliptic ($Q < 0$) and hyperbolic ($Q > 0$) domains, independently of the dynamical nature of the elliptic regions (vortex cores or negative-Q regions in the background

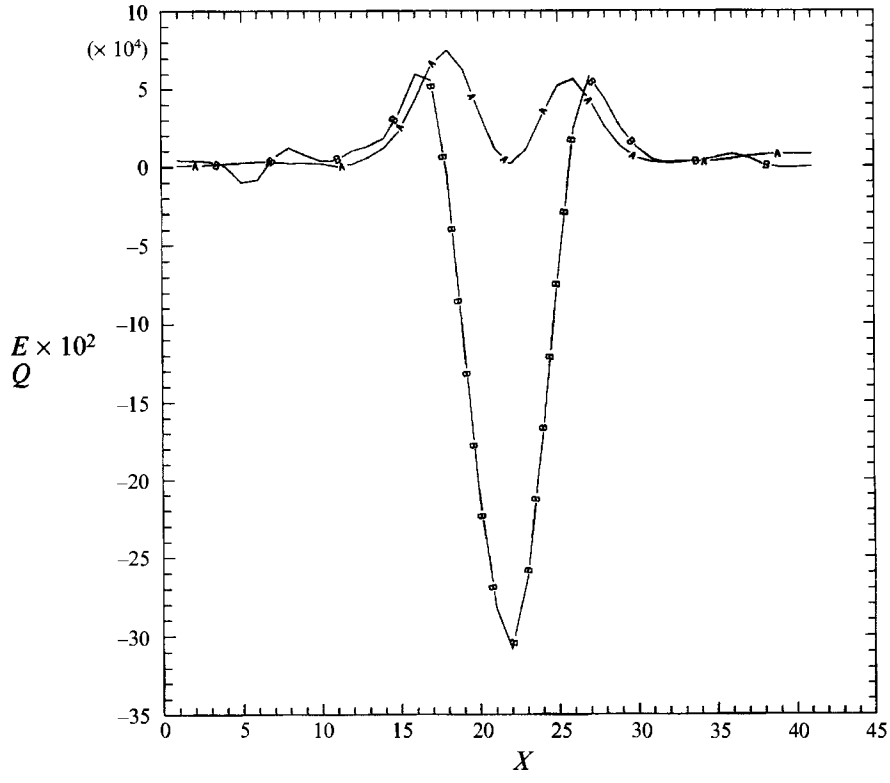

FIGURE 3. Cross-section of the energy (curve A) and of Q (curve B) in a typical two-dimensional coherent structure and in its surroundings. The abscissa is given in grid spacings. The vortex considered here is the coherent structure centred approximately on the grid point (100, 85), in the upper right of figure 1.

turbulent field) or of the hyperbolic domains. However, figures 1 and 2 illustrate how regions with the same sign of Q may have a very different structure: For example, the strong hyperbolic regions which we have called circulation cells usually surround the coherent structures and behave as organized domains at the periphery of the vortex cores; their dynamical role is quite different from that of hyperbolic patches inside the background turbulence. In fact, the study of chaotic advection in two-dimensional turbulence (Babiano *et al.* 1993) has shown that the values of the Lagrangian Lyapunov exponents are different in the circulation cells and in hyperbolic patches in the background turbulence: in this case, a partitioning of the two-dimensional turbulence in terms of both Q and E is necessary.

A detailed view of the energy ($E \times 10^2$) and of the Q-distribution in a coherent structure and in its surroundings is given in figure 3, which shows a cross-section of these fields for the large coherent structure visible in figure 1(a, b) centred approximately on the grid point (100, 85). For a coherent structure, the maximum of the energy is attained at scale D_I corresponding with the isoline $Q = 0$, which defines the boundary of the vortex core. Inside the isoline $Q = 0$, the value of Q rapidly decreases towards the minimum $Q \approx -\omega^2$ which is attained in the proximity of the vortex centre where the deformation is very small and an almost solid-body rotation is observed. Outside the isoline $Q = 0$, the value of Q reaches a positive maximum in the entrainment region where deformation dominates rotation. This domain is the

well-structured circulation cell surrounding the vortex core. In this region, the energy decreases from the maximum values, attained in the proximity of the isoline $Q = 0$ which may be considered as the boundary of the vortex core, towards the small values encountered in the background turbulence. This allows three basic topological domains of two-dimensional turbulence to be defined.

(i) The background turbulent field. This is a region characterized by low energy and moderate values of Q oscillating between positive and negative values, say $E < E_0$ and $-Q_0 < Q < Q_0$, where E_0 and Q_0 are appropriately defined energy and Q thresholds. The background turbulence is a mixture of elliptic and hyperbolic regions.

(ii) The circulation cells at the periphery of coherent structures. These are strongly hyperbolic regions where $Q \gg Q_0$ and $E > E_0$.

(iii) The vortex cores. These are strongly elliptic domains where $Q \ll -Q_0$. Clearly, the centres of the vortices are characterized by low energy.

For the turbulent field displayed in figure 1, an indicative energy discriminator between the circulation cells and the background turbulence is the value $E_0 \approx 30$ (in dimensionless units) and the maximum energy of the circulation cells is fixed at about $E_m \approx 200$. Values of Q above the threshold $Q_0 = 10^4$ (in dimensionless units) are associated with the circulation cells while values of Q less than $-Q_0$ are found in the vortex cores. In the background turbulent field, the absolute value of Q is much smaller ($-Q_0 < Q < Q_0$) and the energy is less than E_0. In this domain, the spatial distribution is dominated by regions with positive values of $Q (0 < Q < Q_0)$. The strong jump in the value of Q between the 'inside' of a vortex and the surrounding circulation cell is clear evidence of the coherent nature of the vortices.

Clearly, even the above partitioning technique produces just a rough approximation of the topology of two-dimensional turbulence. For example, if the elliptic and hyperbolic domains display self-similar properties, then these may be hidden by the above parametrization because elliptic and hyperbolic domains are mixed in region (i). In addition, the values of the energy and Q thresholds separating the various regimes may vary from one turbulent field to another. In the present work we show that single-particle dispersion, contrary to chaoticity properties, may be appropriately understood in terms of the dominance of hyperbolic or elliptic regions, without the need of adding an energy criterion. This may well be due to the peculiar behaviour of advected particles which usually avoid strongly elliptic regions.

3. Single-particle dispersion: definitions and experimental illustration

3.1. *Definition*

The study of Lagrangian particle dynamics is herein based on the analysis of single-particle dispersion. The single-particle dispersion A^2 of an ensemble of advected particles is defined as

$$A^2(\boldsymbol{a}(t'), t) = \langle (\boldsymbol{x} - \boldsymbol{a}(t')) \cdot (\boldsymbol{x} - \boldsymbol{a}(t')) \rangle_a, \tag{4}$$

where $\boldsymbol{x}(\boldsymbol{a}, t)$ is the position of an advected particle at time t, $\boldsymbol{a}$ is its Lagrangian coordinate at time t' (taken as the time origin) and $\langle \cdot \rangle_a$ is an ensemble average over all particles (i.e. all values of $\boldsymbol{a}$). The value of $\boldsymbol{a}$ is used as a label of the particle. If the turbulence is homogeneous, the dependence of the single-particle dispersion on $\boldsymbol{a}$ and/or t' is negligible. In the more general case, the single-particle dispersion depends on the dynamics properties of the characteristic domains of the turbulent field.

The single-particle dispersion (4) is a Lagrangian characteristic related to the Lagrangian velocity autocorrelation function and to the Lagrangian energy spectrum.

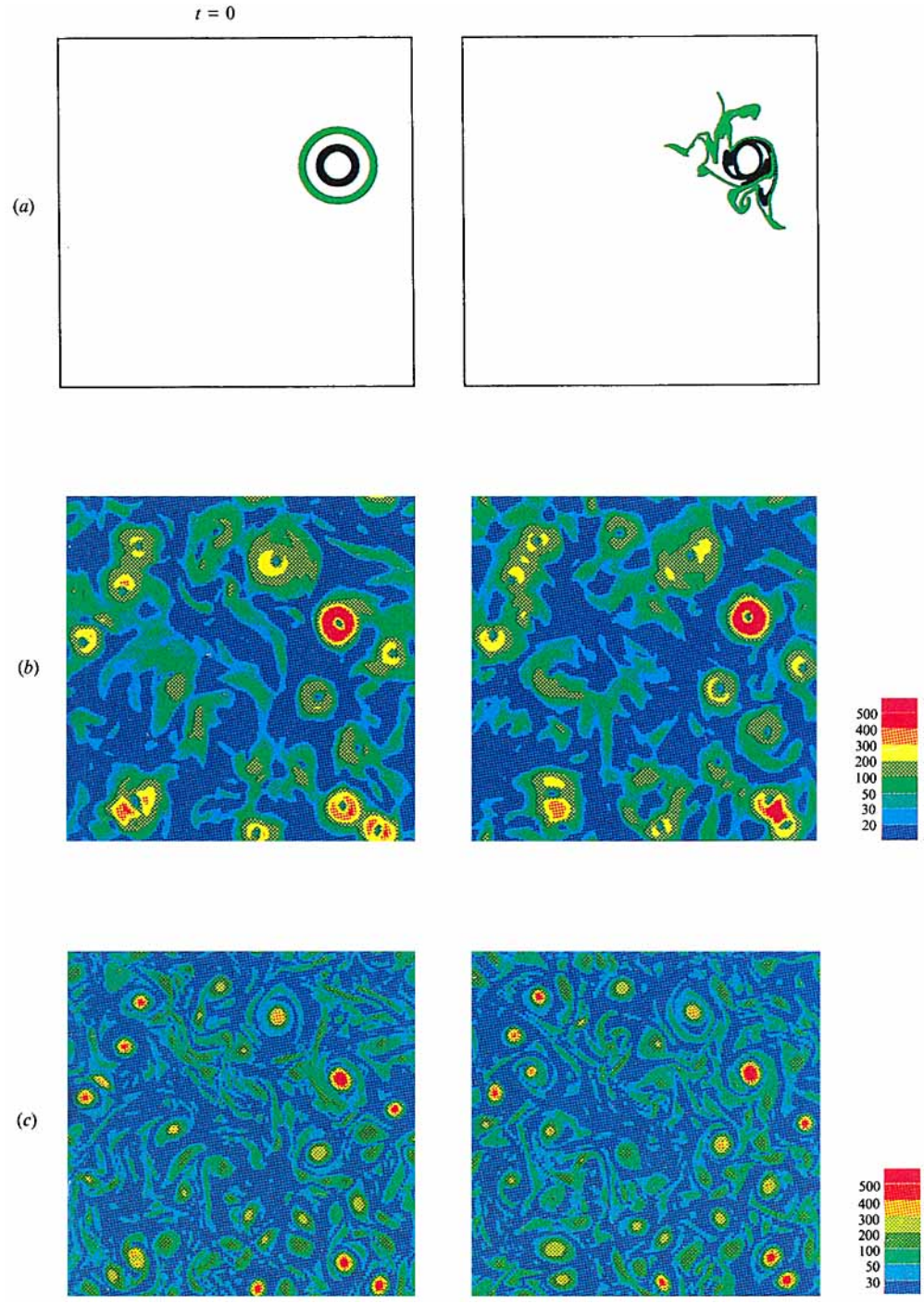

FIGURE 4. For caption see facing page.

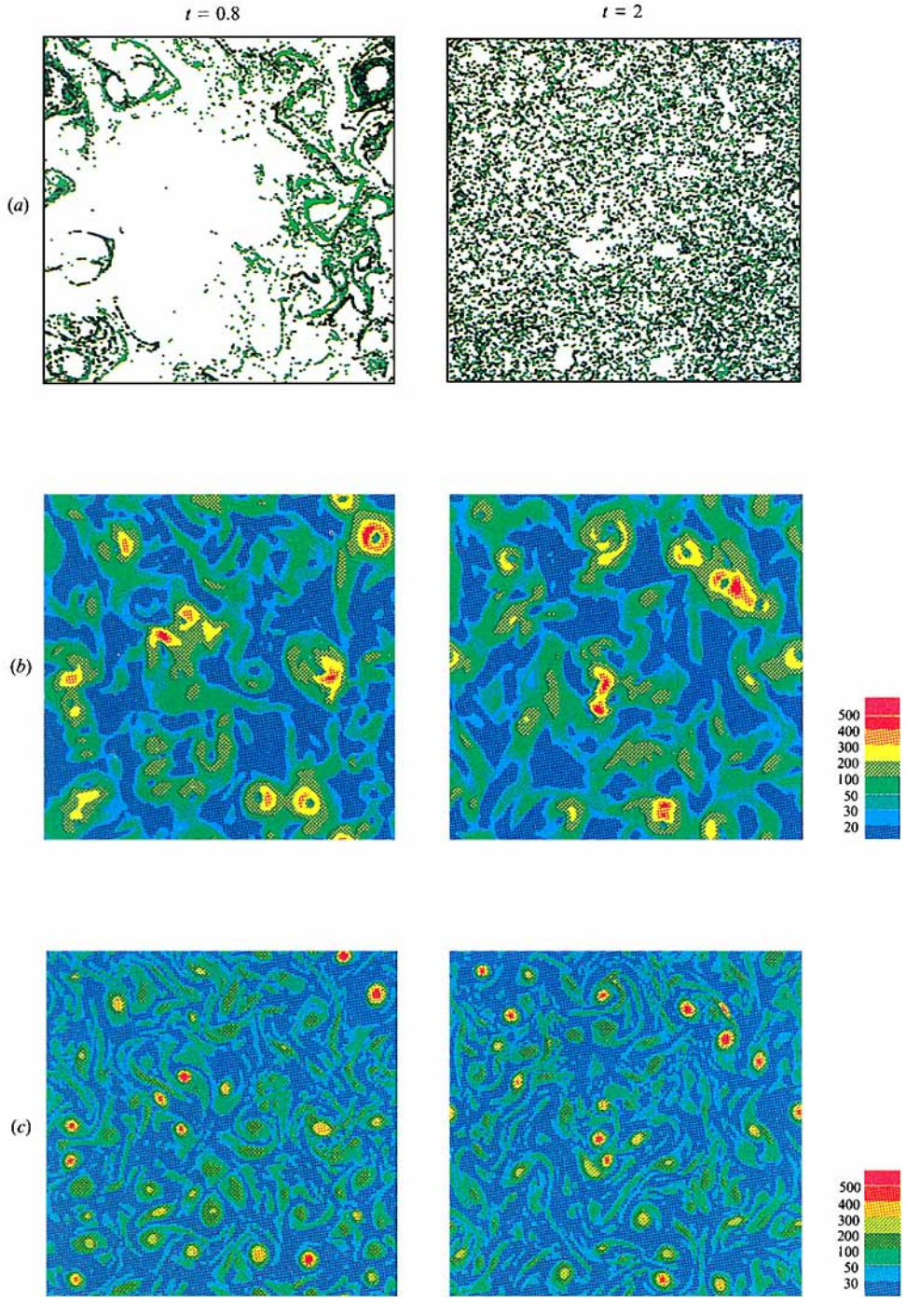

FIGURE 4. Time evolution of (*a*) the particle distribution, (*b*) Eulerian energy, and (*c*) Eulerian vorticity levels. The four images correspond to the times $t = 0$, $t = 0.1$, $t = 0.8$ and $t = 2$. Particles in the inner ring C1 are coloured black while particles in the outer ring C2 are coloured green.

The single-particle dispersion at both small and large times can be obtained by the Taylor (1921) theorem. In this context, (4) yields the following asymptotic behaviour:

$$A^2(\boldsymbol{a}, t) \approx 2\mathscr{E}t^2 \quad \text{when } t \to 0, \tag{5}$$

$$A^2(\boldsymbol{a}, t) \approx 2Kt \quad \text{when } t \to \infty, \tag{6}$$

where $\mathscr{E} = \frac{1}{4}\langle \| \boldsymbol{V}(\boldsymbol{a}, t')\|^2 + \| \boldsymbol{V}(\boldsymbol{a}, t)\|^2 \rangle_{\boldsymbol{a}}$ is the mean Lagrangian kinetic energy, $\boldsymbol{V}(\boldsymbol{a}, t)$ is the Lagrangian velocity of the particle $\boldsymbol{a}$ at time t and K is the eddy diffusivity (all these definitions can be generalized to tensor notation).

The above asymptotic results have recently been extended by Babiano *et al.* (1987*b*), by considering the natural link between the single-particle dispersion and Lagrangian energy spectrum. For stationary and homogeneous Lagrangian statistics characterized by a Lagrangian energy spectrum $P(\nu) \approx \nu^{-n}$, where ν is the (Lagrangian) frequency, the dominant behaviour of the single-particle dispersion is

$$A^2 \sim t^2 \quad \text{for} \quad n > 1, \tag{7}$$

$$A^2 \sim t^{n+1} \quad \text{for} \quad -1 < n < 1. \tag{8}$$

From (7), (8) one can see that: (i) the behaviour (5) no longer depends on the slope of the Lagrangian energy spectrum; and (ii) the signature of the asymptotic Brownian regime (6) is a flat Lagrangian energy spectrum ($n \approx 0$). The important conclusion is that the robustness of the behaviour (5), (6) allows the dispersion properties to be disconnected from the rather restrictive hypothesis of homogeneity. This fact is in complete agreement with the statistical results furnished by the analysis of Lagrangian data from non-homogeneous oceanic and atmospheric velocity fields where the behaviour (5), (6) is systematically observed. In addition, (8) allows the existence of anomalous diffusion regimes at intermediate times linked with a spectral index $n \neq 0$. In this regard, we recall that recent studies of drifter dynamics have detected a regime of anomalous diffusion $A^2 \propto t^{1.6}$ linked with a Lagrangian energy spectrum $P(\nu) \approx \nu^{-0.6}$ (Osborne, Kirwan & Provenzale 1989; Sanderson, Goulding & Okubo 1990; Provenzale *et al.* 1991; Sanderson & Booth 1991). The dynamical origin of this regime is still unclear; analogously, it is unclear which is the value of the time delay required for the drifter absolute dispersion to become Brownian-like.

The asymptotic behaviour (5) and (6) is classically derived in the limit of timescales which are respectively much smaller or larger than the Lagrangian integral timescale T_L. The large-time dispersion regime is usually observed for time delays which are also much larger than an appropriate Eulerian decorrelation time T_E; after this time the increments in the particle trajectory become independent of each other and a classic Brownian motion may be observed, independent of the turbulent topology. Anomalous diffusion at asymptotically larger times may be observed only for a divergent T_E. At the other end of the timescale, at very short times the particle trajectories are comparable to ballistic motions, and the classic form $A^2 \propto t^2$ depends only on energy level. At intermediate times (e.g. $T_L < t < T_E$), a dynamical regime different from the asymptotic behaviour (5), (6) may be present. These times are excluded from the classical analysis based on the Taylor theorem; nevertheless, intermediate times are often the relevant ones from the point of view of practical applications.

3.2. *Experimental illustration of a dispersion process*

In figure 4 we show an illustration of the particle distribution and of the energy and vorticity levels for a typical dispersion experiment. The Eulerian field considered here

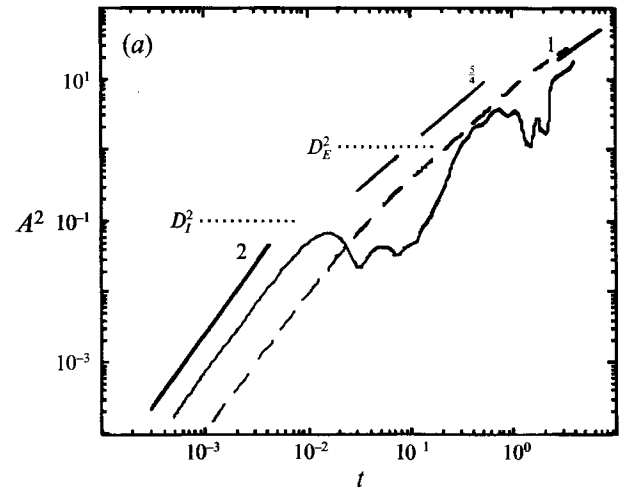

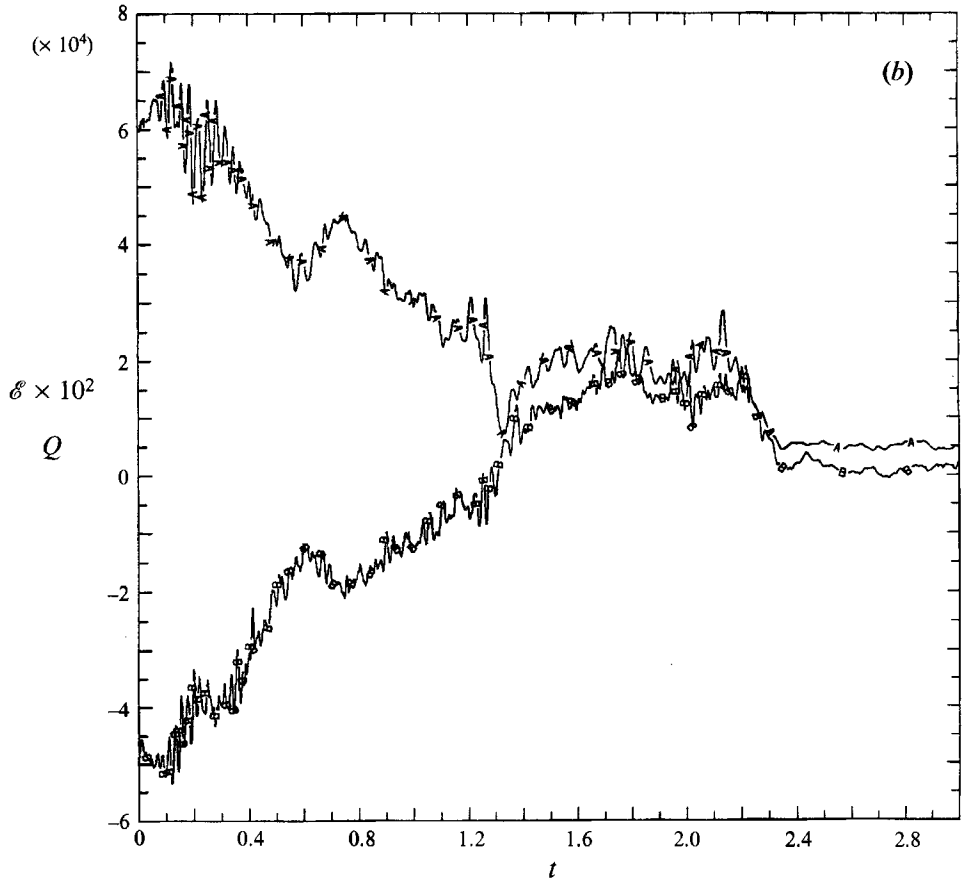

FIGURE 5. (*a*) The global single-particle dispersion A^2 for the initial sowing in a coherent structure (solid curve), and for a regular sowing in the entire domain (dashed curve). (*b*) The time evolution of the mean Lagrangian kinetic energy (curve A) and of the mean value of Lagrangian Q (curve B); the averages are taken over the trajectories of the particles sown in the proximity of the isoline $Q = 0$.

is R128F10. The various panels of figure 4 show the Eulerian field and the particle distribution at times $t = 0$, 0.1, 0.8, and 2. As mentioned above, high energy and vorticity levels are correlated with the action of coherent structures while low energy and vorticity levels, represented in dark blue, are found in the background turbulent field. The medium energy levels, represented in green, may on average be correlated with the circulation cells at the vortex peripheries. The circulation cells are physically composed of the portions of the background field which are carried by isolated vortices and by the regions of close vortex interactions. In this experiment, two ensembles of 6000 particles were initially placed in two rings C1 and C2 outside the isoline $Q = 0$ of the vortex shown in figure 3. The two rings are centred in the vortex epicentre; the outer radii are equivalent to 8 and 12 grid intervals for C1 and C2 respectively, the inner radii are equivalent to 6 and 10 grid intervals respectively.

Panels (a, b, c) of figure 4 show that the particles disperse towards low or medium energy and vorticity levels. High-vorticity domains and active coherent stuctures clearly display a great impermeability to inward particle fluxes from outside regions. At large dispersion times ($t = 2$), the particle distribution is rather homogenized, even though the majority of coherent vortices are still visible, being characterized by an almost complete lack of trapped particles deep inside them. The results shown in figure 4 confirm that passive particles cannot penetrate the inner core of existing coherent structures.

At intermediate times ($t = 0.8$), figure 4 shows that the advected particles tend to concentrate in the circulation cells surrounding the coherent structures. This is observed for circulation cells corresponding to different vortices, not just for the circulation cell surrounding the vortex where the particles were initially seeded. These results indicate that these highly hyperbolic regions at the periphery of vortex cores seem to be preferred by neutral particles, which, by contrast, tend to avoid strongly elliptic regions. Note, in particular, that the circulation cells are domains where the vorticity is very small. In fact, the tendency of passively advected neutral particles to concentrate in the proximity of the isolines $\omega = 0$ is a more general result: as it is shown below, even though at large times the particle distribution is apparently homogenized, there is always a significant concentration of the neutral particles in the proximity of the $\omega = 0$ isolines in the background turbulent field.

3.3. *Particle traps and circulation cells*

We now analyse in detail the single-particle dispersion properties for two different initial conditions on the particle distribution. We consider the dispersion from an isolated vortex, and the dispersion from a regular sowing in the entire domain. The cloud in the vortex is composed of 4000 particles, sown in groups of 100 on 40 different vorticity isolines where $Q < 0$. The regular sowing is composed of 8000 particles initially deployed on a regular grid in $(2\pi, 2\pi)$.

Figure 5(*a*) shows the single-particle dispersion (4), averaged over all particles, for an initial sowing in the isolated vortex shown in figure 3 (solid curve) and in the entire domain (dashed curve). Figure 5(*b*) shows the evolution of Q and of the Lagrangian kinetic energy $\mathscr{E}(\mathscr{E} \times 10^2)$ as obtained by an average over the particles sown on a vorticity isoline in the vicinity of the isoline $Q = 0$ for the vortex. The isoline $Q = 0$ may be considered as the boundary of the vortex core; we denote these particles by $\boldsymbol{a}_0$. The single-particle dispersion from the vortex can be described in four distinct phases. First (phase I: $t < 0.2$, $Q < 0$), the particles disperse in the vortex and remain trapped inside it. The small-time asymptotic law (5) is obeyed until the particles undergo regular oscillations determined by the diameter of the vortex D_I. This corresponds to

the flattening of the absolute dispersion between about $t = 0.01$ and $t = 0.2$. The trapping episodes last for about $t - t' \approx 40\overline{T}_L$. In this phase, the values of the kinetic energy and of Q of the $\boldsymbol{a}_0$ particles are approximately constant. In the second phase (phase II: $0.2 < t < 1$, $Q < 0$), the particles are rapidly ejected from the vortex core. The value of the kinetic energy of the $\boldsymbol{a}_0$ particles decreases while the values of Q show a regular increase. In the third phase (phase III: $1 < t < 2$, $Q > 0$), the particle dispersion from the vortex is slowed down again since the particles are trapped in the circulation cell surrounding the vortex (second knee in the absolute dispersion curve). The circulation cells are characterized by the most energetic scale D_E, which represents an upper bound to the inverse energy cascade (Babiano & Zouari 1993). During this phase, the particles $\boldsymbol{a}_0$ are characterized by values of $\mathscr{E} \approx E_m$ and $Q > 0$ since deformation dominates rotation. This phase is quite long and it is characterized by a certain degree of stationarity. In spite of these traps, however, the particles are progressively pushed towards low-vorticity isolines. In the final phase (phase IV: $t > 2$, $Q > 0$ and $Q < 0$), the particles reach the background turbulent field; at asymptotically large times the dispersion process may be described in terms of the Brownian dispersion (6).

The behaviour of the particles $\boldsymbol{a}_0$ may be strictly related to the topology defined in §2. In particular, one may note that the circulation cell at the periphery of the vortex core ($Q \gg 0$) is a region of particle trapping where neutral particles may reside for a long time (trapping times of the order of 30 $\overline{T}_L$). Conversely, the absolute dispersion from a regular particle sowing (dashed curve in figure 5*a*) does not display any trapping phase. In this case, one may see that the observed dispersion law is an average of the different dispersive phases described above, i.e. an average of the contributions coming from both the elliptic and hyperbolic regions. The average dispersion for the regular particle sowing displays an intermediate dispersion phase characterized by a power law $A^2 \propto t^\alpha$ with $\alpha \approx \frac{5}{4}$ for times between about $t = 0.1$ and $t = 1$. An obvious question at this point concerns the origin and universality of the power-law behaviour observed above, as well as a detailed understanding of the role of the different topological domains in the particle dispersion process. To answer this question, in the following we introduce a normalization of the Q-values which allows better separation of the various contributions of the turbulent fields to the particle dynamics.

3.4. *Normalization of the elliptic and hyperbolic regions*

In general, the precise values of Q-thresholds separating the different dispersion phases described above vary from one turbulent field to another. Analogously, the variance Q-fields with respect to the average values may also vary depending upon the situation considered. To circumvent this difficulty, from (1) to (3) we define a normalized value of the parameter Q as

$$Q^* = \frac{Q}{2\|\nabla \boldsymbol{U}\|^2} = \frac{s^2 - \omega^2}{s^2 + \omega^2}. \tag{9}$$

The parameter Q^* maintains the same sign as Q (negative in elliptic domains and positive in hyperbolic regions); however, the amplitude of Q^* is normalized between -1 and $+1$. Inside strongly elliptic regions ($Q < 0$, $s^2 \approx 0$), $Q^* \to -1$; conversely, in strongly hyperbolic domains ($Q > 0$, $\omega^2 \approx 0$), $Q^* \to 1$. A value $Q^* \approx -1$ characterizes both the strong vorticity concentrations inside the coherent structures and those regions of the background turbulence where the deformation is almost absent. A value $Q^* \approx 1$ characterizes the circulation cells surrounding the coherent structures and those regions of the background turbulence where $\omega \approx 0$. In the following, we show

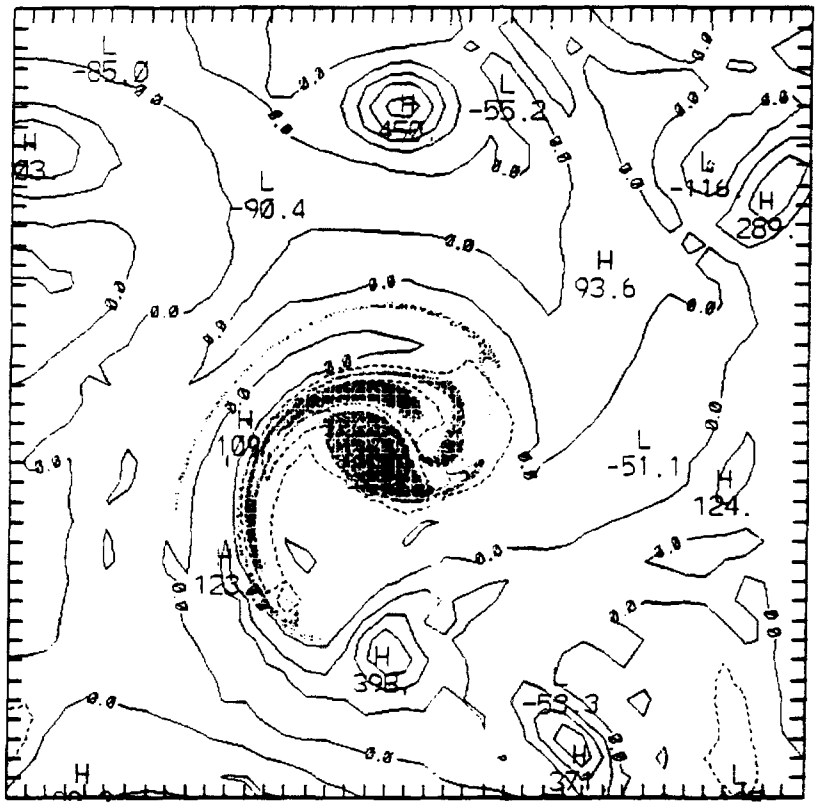

FIGURE 6. Isolines of the vorticity field and distribution of neutral particles at an instant during the interaction between two coherent structures. The passive particles were initially sown inside each one of the two vortices. The vortex interaction induces a filamentation of the vorticity field and the subsequent ejection of some of the particles. The particle distribution shows that the distribution of ejected particles follows quite closely the isoline $\omega = 0$.

that passively advected neutral particles display a neat tendency to concentrate in regions where $Q^* \approx 1$.

In figure 4, we have shown that during the dispersion process neutral particles concentrate in the circulation cells around the coherent structures; in these regions, the vorticity levels are quite small and $Q > 0$ (see the particle distribution at $t = 0.8$, for example). Figure 5(*b*) confirms that these regions are domains of particle trapping. These regions are characterized by values of Q^* close to 1 owing to the small values of ω. For large dispersion times ($t = 2$, figure 4), owing to the increasing attraction of the particles towards the background turbulence the particle distribution is homogenized. This latter domain is characterized by small (positive and negative) values of ω; the network of isolines $\omega = 0$ thus constitutes what may be called the support of the background turbulent field. Clearly, $Q^* \approx 1$ in the proximity of $\omega = 0$.

The correlation between the passive particle dynamics and the isolines $\omega = 0$ is further illustrated in figure 6, which shows the interaction between two coherent structures as visualized by the isolines of the vorticity field and by the distribution of passive particles initially sown inside each one of the two vortices. The vortex interaction induces a filamentation of the vorticity field and the subsequent ejection of some of the particles. The figure shows that the distribution of ejected particles follows

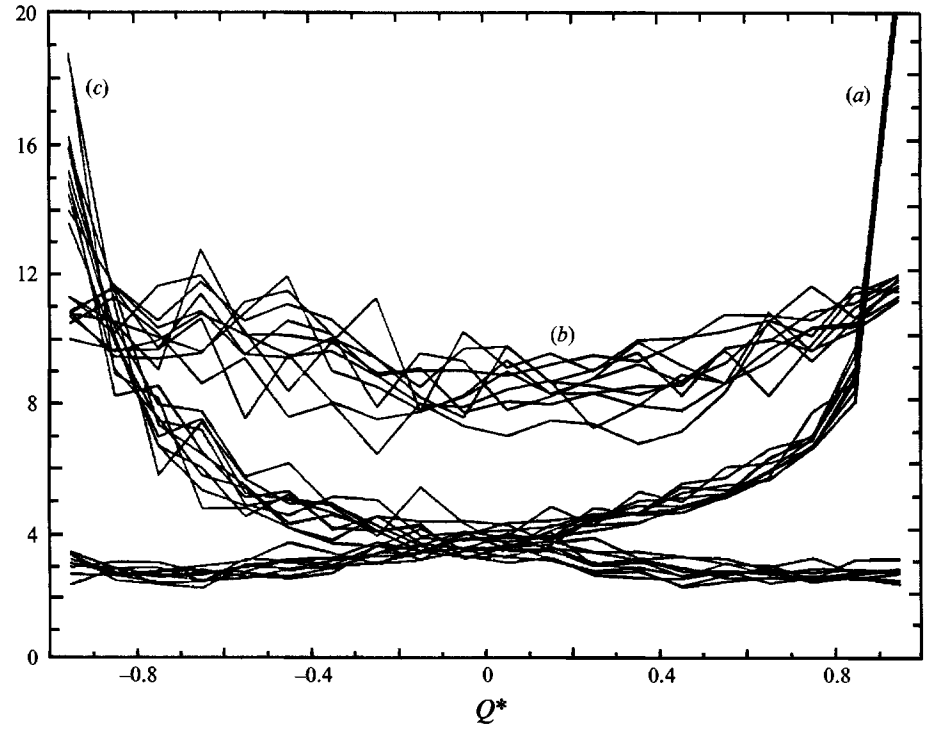

FIGURE 7. Distribution of the number of particles N_p, of the Lagrangian mean energy and of $2\|\nabla U\|^2$ as functions of Q^*, for different times. Curves (*a*) show the percentage of particles ($10^2 \times N_p/N_{tot}$, where $N_{tot} = 8000$ is the total number of particles); curves (*b*) report the normalized Lagrangian kinetic energy $E/\bar{E}$ where $\bar{E} = 53.5$; curves (*c*) report $2\|\nabla U\|^2/\bar{Z}$ where $\bar{Z} = 2600$. Different curves in each group correspond to different times.

the isoline $\omega = 0$ quite closely. During this process, the mean velocity of the advected particles is almost parallel to the isoline $\omega = 0$, even though the velocity field is non-stationary. This happens in both the circulation cells and the background turbulence; in both cases, the topology is characterized by $Q^* \approx 1$. These two types of hyperbolic regions are quite different from an energetic point of view; however, in both these deformation-dominated domains the mean velocity turns out to be parallel to the isolines $\omega = 0$, and the advected particles tend to follow these isolines. This behaviour is consistent with the results obtained by Babiano *et al.* (1987*a*) on the dynamics of passive scalar tracers in two-dimensional turbulence.

3.5. *Statistical weight of the elliptic and hyperbolic domains*

Given the parametrization of the turbulent field in terms of Q^*, we may now evaluate the statistical weight of the different topological domains in the dispersion law observed for a regular sowing (dashed curve in figure 5*a*). Figure 7 shows the distribution of the number of particles N_p, of the Lagrangian mean energy and of the quantity $2\|\nabla U\|^2$ defined by (1) as functions of Q^*, for different times. Curves (*a*) show the percentage of particles ($10^2 \times N_p/N_{tot}$, where $N_{tot} = 8000$ is the total number of particles), curves (*b*) report the Lagrangian kinetic energy normalized by the mean turbulent kinetic energy $\bar{E} = 53.5$ ($E/\bar{E} \times 10$), and curves (*c*) report $2\|\nabla U\|^2$ normalized by the enstrophy of the field, $\bar{Z} = 2600$. Different curves in each group correspond to different times.

As a first observation, we note that the results reported in figure 7 indicate that all the quantities defined above are statistically stationary during the dispersion process. The shape of the distribution of N_p quantitatively confirms that passively advected neutral particles tend to sample preferentially regions where $Q^* = 1$. In the present case, the particles have been uniformly seeded in all the domain and even at time $t = 0$ they preferentially sample the hyperbolic regions. This is because these regions occupy the largest portion of the turbulent flow. In the case of particles seeded only in elliptic regions where $Q^* < 0$, the curve $N_p(Q^*)$ evolves with time and it asymptotically attains the shape shown in figure 7. These findings agree with the results reported by Babiano *et al.* (1987*a*) and by Ohkitani (1991), which already indicated the tendency of passive scalar tracers and passive neutrally buoyant particles in two-dimensional turbulence to evolve into those regions of the turbulent field characterized by small vorticity levels.

The results reported in figure 7 also indicate that the average kinetic energy of the advected particles is approximately independent of the value of Q^*. This should have been expected since Q^* is not a good energy discriminator. Clearly, every time dynamical behaviour is well parametrized by the value of Q^*, then a parametrization in terms of the Lagrangian kinetic energy is scarcely useful. This seems to be the case for the average properties of the dispersion of passive tracers, where a three-region segmentation such as that discussed in §2.2 should probably be of limited interest and the parametrization in terms of Q^* is more enlighting. On the other hand, if one is interested in the behaviour of insulated vortices, or in the dynamics of circulation cells as opposed to that in the background turbulence, then a segmentation based on the values of both Q^* and $E/\bar{E}$ is appropriate. This indicates that the proper parametrization is probably not an absolute choice but it is, rather, dependent on the type of question to be answered. In the next section we consider this problem again in the framework of absolute dispersion at intermediate times. As a final remark, we note that the dependence of $2\|\nabla U\|^2$ on Q^* is almost opposite to that of N_p; this result indicates that the regions where the particle concentration is large are characterized by small velocity gradients.

From the above results on the dependence of N_p on Q^*, we may conclude that the dispersion law displayed in figure 5(*a*) (dashed curve) is dominated by the strongly hyperbolic regions where $Q^* \approx 1$. However, since the average kinetic energy is approximately independent of Q^*, the dominance of the regions with $Q^* \approx 1$ does not modify the small-time asymptotic behaviour (5), which depends only on the energy of the turbulent field. An important question, then, concern the respective effects of the hyperbolic and of the elliptic regions on the dispersion properties at intermediate times, as well as their effect on the long-time asymptotic law (6). In the next section we consider the first question, while the long-time asymptotic behaviour will be left to a future work.

4. The intermediate dispersion phase: experimental results

In this section, we examine the effects of the elliptic and hyperbolic regions on the properties of absolute dispersion (4) at intermediate times. To this end, here we explicitly consider the two types of Eulerian fields mentioned in §2, namely R128F10 and R512F40. In all the experiments considered here, we have integrated the Lagrangian motions of 8000 particles which have been initially sown on a regular grid in the entire domain. The Lagrangian time step for the numerical integration of the particle motion is equal to the Eulerian time step of the model; however, the

Lagrangian parameters (particle positions, velocities etc.) have been recorded only at $N_s = 2000$ and $N_s = 1600$ time instants for the R128F10 and R512F40 experiments respectively. The time steps between two successive Lagrangian recording are thus $\Delta t_s = 0.003$ and $\Delta t_s = 0.00025$ for the two experiments.

4.1. *Definition of conditional averages*

The absolute dispersion curve shown in figure 5(*a*) has been obtained by an unconditioned average over all the advected particles. In order to disentangle the role of the different topological domains on the particle dispersion processes, here we define appropriate conditional averages which identify 'topologically homogeneous' subsets $\boldsymbol{a}'$ of advected particles. The conditional averages are defined by appropriate constraints on the sign and/or the amplitude of Q^*. Quantitatively, we define

$$A_c^2(t) = \langle (\boldsymbol{x} - \boldsymbol{a}(t')) \cdot (\boldsymbol{x} - \boldsymbol{a}(t')) \rangle_{\boldsymbol{a}'}, \tag{10}$$

where $t = t' + im\Delta t_s$, $t' = 0$, $i = 1, 2, \ldots, N_s/m$; m determines the time discretization of the statistical treatment. At each value of t, the set of particles $\boldsymbol{a}'$ considered in the evaluation of $A_c^2(t)$ are selected such that the quantity

$$\overline{Q^*} = \frac{1}{t - t_0} \int_{t_0}^{t} Q^*(\boldsymbol{a}, s)\, \mathrm{d}s \tag{11}$$

verifies the requirement

$$\overline{Q^*} < 0 \quad \text{or} \quad \overline{Q^*} > 0, \tag{12}$$

and/or

$$Q_1^* < \overline{Q^*} < Q_1^* + \Delta Q^*, \tag{13}$$

where $-1 < \overline{Q^*} < 1$ and Q_1^* is a value of Q^* chosen as a threshold. The time t_0 is an appropriate defined instant of time between the time origin t' and the current time t; t_0 defines the restrictivity of the conditional average. With (11)–(13), we will evaluate the absolute dispersion (10) with two different choices of t_0:

$$t_0 = t - im\Delta t_s, \tag{A I}$$

$$t_0 = t - m\Delta t_s. \tag{A II}$$

With (A I), the ensemble average (10) is defined at each time t only over those particles $\boldsymbol{a}'$ for which the condition on $\overline{Q^*}$ is verified over the entire trajectory from t' to t. It is a quite restrictive selection of the set $\boldsymbol{a}'$ which retains only those particles which have evolved, in a time-average sense, in the same topological domain from t' to t. With (A II), the selection rule is less restrictive: in fact, here it is necessary only that the condition on $\overline{Q^*}$ be verified in the individual time interval $m\Delta t_s$ immediately before the time t, independent of the past history of the particle between t' and t_0. In this latter case, the statistics are strictly representative of the topological domain under study only if $t - t_0$ is larger than the Lagrangian decorrelation time T_L, owing to the mixing of different particles allowed by this type of conditional average. In the following, we will consider both types of conditional averages (A I and A II) and different choices of m ($m = 1$, $m = 10$ for R128F10 and $m = 1$, $m = 8$ for R512F40). Hereinafter, the absolute dispersion (variance of the particle distribution) is given in units of the number of grid intervals; i.e. if $\Delta x = 2\pi/R$ ($R = 128$ or $R = 512$) is the grid interval, $A_c^2(t) = A_c^2(t)/\Delta x^2$.

4.2. *Dispersion in elliptic and hyperbolic domains*

Figure 8(*a*) shows the absolute dispersion curves of A_c^2 as functions of time, for the simulation R128F10. These curves have been obtained with conditional average (11)–(13) of the type (A I), on the sign and amplitude of $\overline{Q^*}$ with $m = 1$, $\Delta Q^* = 0.1$. The

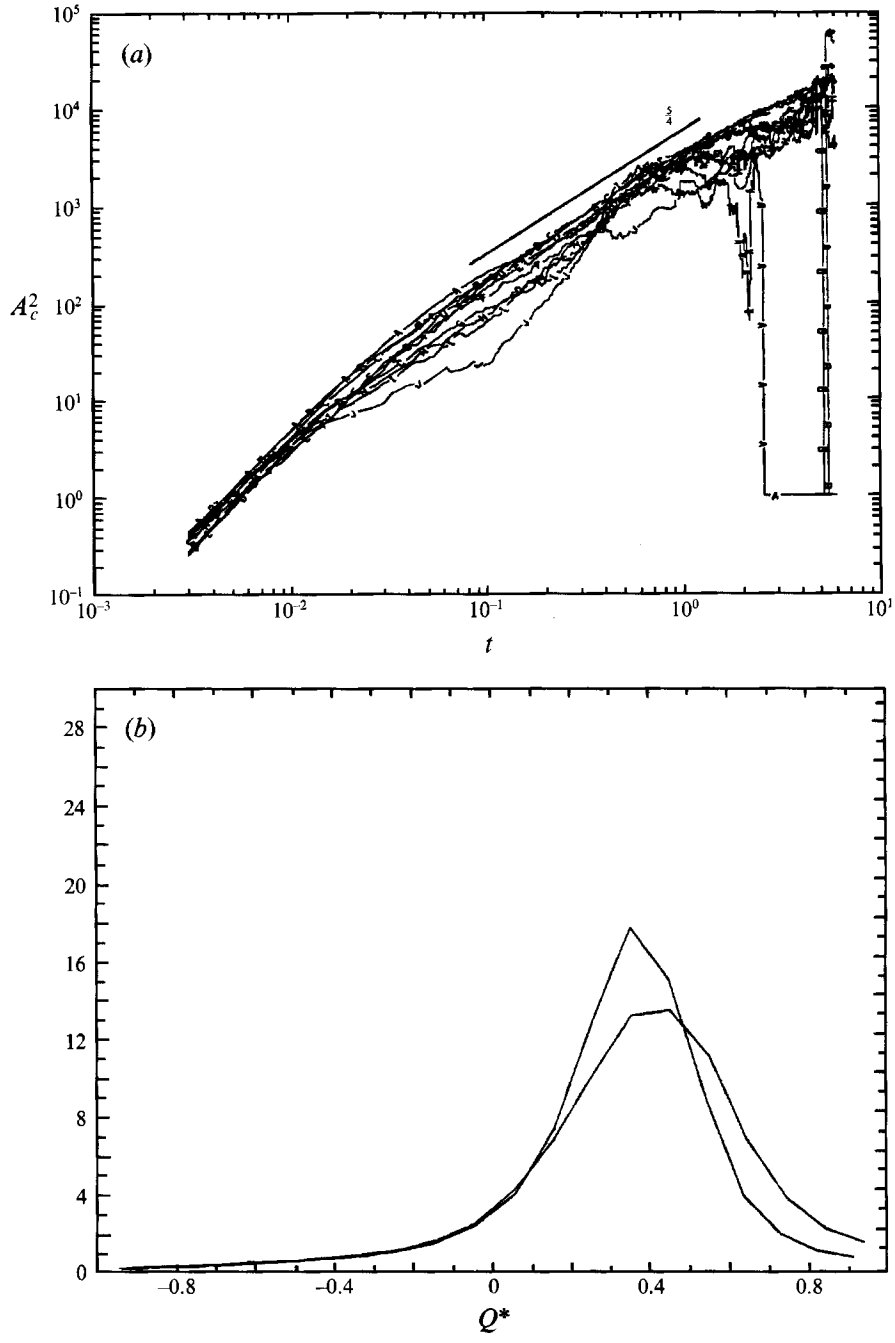

FIGURE 8. (*a*) The absolute dispersion A_c^2 versus time, for the simulation R128F10. The various curves have been obtained by the conditional average (11)–(13) of the type (A I) and represent the absolute dispersion as averaged over the particles that have evolved, for all times between t' and t, in the domains characterized by $0.9 < \overline{Q^*} < 1$ (A), $0.7 < \overline{Q^*} < 0.8$ (B), $0.6 < \overline{Q^*} < 0.7$ (C), $0.2 < \overline{Q^*} < 0.3$ (D), $0 < \overline{Q^*} < 0.1$ (E), $-0.2 < \overline{Q^*} < -0.3$ (F), $-0.6 < \overline{Q^*} < -0.7$ (G), $-0.7 < \overline{Q^*} < -0.78$ (H), $-0.8 < \overline{Q^*} < -0.9$ (I), $-0.9 < \overline{Q^*} < -1$ (J). (*b*) The time-averaged number of particles $N_p \times 10^{-2}$ that have remained inside the same domain (as characterized by a given range of $\overline{Q^*}$ values) for all times between t' and t. The two curves refer to experiment R128F10 and to a similar experiment with a field R512F40.

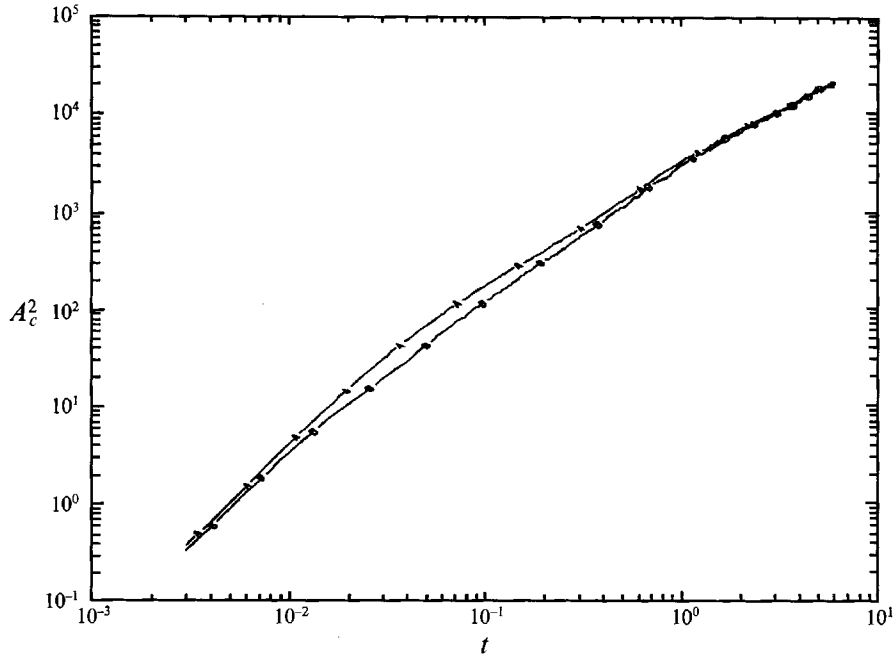

FIGURE 9. Absolute dispersion A_c^2 versus time, for the simulation R128F10, as obtained by the conditional average (11)–(12) of the type (A II). The curves A and B correspond to $\overline{Q^*} > 0$ and $\overline{Q^*} < 0$ respectively.

curves thus represent the absolute dispersion as averaged over the particles that have evolved, for all times between t' and t, in the domains characterized by $0.9 < \overline{Q^*} < 1$ (A), $0.7 < \overline{Q^*} < 0.8$ (B), $0.6 < \overline{Q^*} < 0.7$ (C), $0.2 < \overline{Q^*} < 0.3$ (D), $0 < \overline{Q^*} < 0.1$ (E), $-0.2 < Q^* < -0.3$ (F), $-0.6 < \overline{Q^*} < -0.7$ (G), $-0.7 < Q^* < -0.8$ (H), $-0.8 < Q^* < -0.9$ (I), $-0.9 < \overline{Q^*} < -1$ (J). The number of particles a' that are retained in the conditional averages for the various intervals of $\overline{Q^*}$ and the various values of t may be quite small or even vanishing; this produces the irregularities observed at large times (in the Brownian regime) for examples in curves A and B.

For small dispersion times, the asymptotic behaviour (5) is well verified, with a proportionality factor (given by the Lagrangian kinetic energy) which is almost independent on the value of $\overline{Q^*}$. The Lagrangian kinetic energy is close to the value of the mean kinetic energy $\bar{E}$, in agreement with the results reported in figure 7. At intermediate times, the dispersion law in the hyperbolic domains ($\overline{Q^*} > 0$) is proportional to $t^{\frac{5}{4}}$. The dispersion in elliptic domains is characterized by a steeper slope, which is however less effective than for $\overline{Q^*} > 0$ because the small-time ballistic regime (5) has a shorter duration in elliptic regions. We shall come back to the dispersion in elliptic domains in the following. In general, the results reported in figure 8(*a*) confirm that the unconditional average of figure 5(*a*) is dominated by the contributions of the hyperbolic domains, i.e. by the circulation cells at the boundary of the coherent structures and by the regions in the background turbulence in the proximity of the isoline $\omega = 0$. The $t^{\frac{5}{4}}$ behaviour is quite robust and it is observed for all regions characterized by $Q^* > 0$, i.e. for the entire ensemble of hyperbolic regions.

Figure 8(*b*) shows the time-averaged number of particles that have remained inside the same domain (as characterized by a given range of $\overline{Q^*}$-values) during all the times between t' and t. The two curves refer to experiment R128F10 described above and to

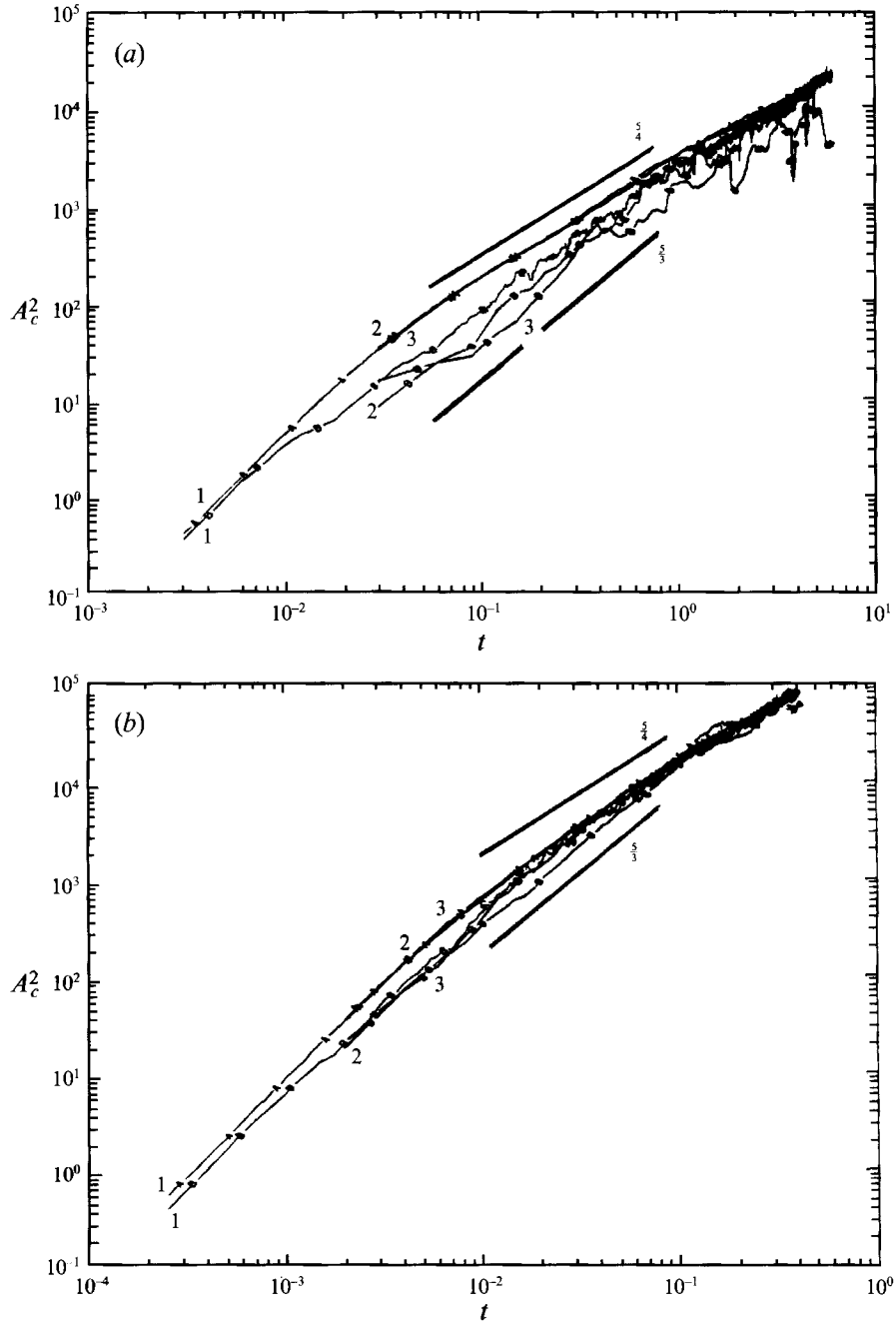

FIGURE 10. The conditional absolute dispersion curves in strongly hyperbolic and strongly elliptic regions for experiments (*a*) R128F10 and (*b*) R512F40. Curves A refer to $\overline{Q^*} > 0.6$ (strongly hyperbolic domains) and curves B to $\overline{Q^*} < -0.9$ (strongly elliptic domains). Curves labelled 1 correspond to a conditional average (A II) with $m = 1$, curves labelled 2 correspond to (A II) with $m = 10$ or $m = 8$, curves labelled 3 correspond to (A I) with $m = 10$ or $m = 8$. The dispersion in strongly hyperbolic regions is very weakly sensitive to the different types of conditional averages. For both R128F10 and R512F40, the $t^{\frac{5}{4}}$ law is clearly confirmed for hyperbolic regions. At intermediate times, the dispersion in strongly elliptic regions (curves B−1, B−2 and B−3) seems to be dominated by an anomalous dispersion law $A_c^2 \propto t^{\frac{5}{3}}$.

a similar experiment with a field R512F40. The two numerical experiments provide similar results. The number of particles that stably remain in the regions where $Q^* < 0$ is quite small, even in the proximity of the value $Q^* \approx -1$. Apparently, this result contradicts the fact that the vortex cores (characterized by $Q^* \approx -1$) are regions for long particle trapping. However, in the case of a regular particle sowing, the number of particles initially placed inside a vortex core cannot be large; in addition, neutral particles are sooner or later irreversibly ejected from the vortex where they are originally placed. The results of figure 8(*b*) thus indicate that the regions with $Q^* < 0$ are not stable domains for neutral particles; in addition, they are domains where the instantaneous concentration of neutral particles is also usually low (recall figure 7). An interesting result concerns the low number of particles which remain stable in the regions where $Q^* \approx 1$. In fact, the instantaneous concentration of particles in these regions is usually large (recall again figure 7). These two results taken together indicate that the turbulent mixing in highly hyperbolic regions is quite active: the instantaneous concentration of neutral particles is large in these regions but their residence time is small, leading to a small number of particles stably remaining in the regions where $Q^* \approx 1$.

From the above results, it is clear that the elliptic and hyperbolic regions induce different properties of the particle dispersion process, concerning both the duration of the ballistic regime (5) and the dispersion properties at intermediate times. In the elliptic regions where $Q^* < 0$, the domain of validity of the small-time asymptotic behaviour (5) is shorter than for the hyperbolic regions where $Q^* > 0$. This indicates that the integral Lagrangian scale T_L is smaller in elliptic regions than in hyperbolic ones. This observation is consistent with the modelization of T_L proposed by Babiano *et al.* (1990), giving $T_L \sim Z^{-\frac{1}{2}}$, where Z is the local enstrophy. The shorter duration of the ballistic regime (5) in elliptic regions induce a loss of effectiveness in particle dispersion in these domains; this is also maintained at intermediate times even though the dispersion law in elliptic regions displays a steeper slope than in hyperbolic regions.

To further confirm the role of the elliptic and hyperbolic regions on the global properties of particle dispersion, we now consider a much less restrictive conditional average, based on requiring $\overline{Q^*} > 0$ and $\overline{Q^*} < 0$. The conditional average is obtained by using (11), (12) and (A II) with $m = 1$. Because $m = 1$, the selection criterion is almost instantaneous. The value of $\overline{Q^*}$ is defined on a time interval $\Delta t_s = 0.003$; this time interval is much shorter than the corresponding average Lagrangian integral timescale and the conditional average separates the different domains less effectively. The interest of this approach is to explore the robustness of the signature of elliptic and hyperbolic regions on particle dispersion, notwithstanding the mixing effect of the type of conditional averages used here. The conditional absolute dispersion for $\overline{Q^*} > 0$ and $\overline{Q^*} < 0$ are shown in figure 9. A global $t^{\frac{5}{4}}$ behaviour is well verified for $\overline{Q^*} > 0$, even with this less restrictive type of conditional average. For $\overline{Q^*} < 0$, the global dispersion displays a steeper slope; in general, a clear difference between the global dispersion laws for $\overline{Q^*} > 0$ and $\overline{Q^*} < 0$ is detected, confirming the robustness of the signature of the different topological domains on the particle dispersion.

4.3. *Dispersion in strongly elliptic and hyperbolic domains*

We now explore the dispersion law in strongly hyperbolic and strongly elliptic domains. The selection of these domains is obtained by using the conditions $\overline{Q^*} > 0.6$ and $\overline{Q^*} < -0.9$. We have considered a larger $\overline{Q^*}$-interval in hyperbolic regions to take into account the entire structure of the circulation cells. In the following we explicitly consider both experiments R128F10 and R512F40. The value of $\overline{Q^*}$ is defined by (11)

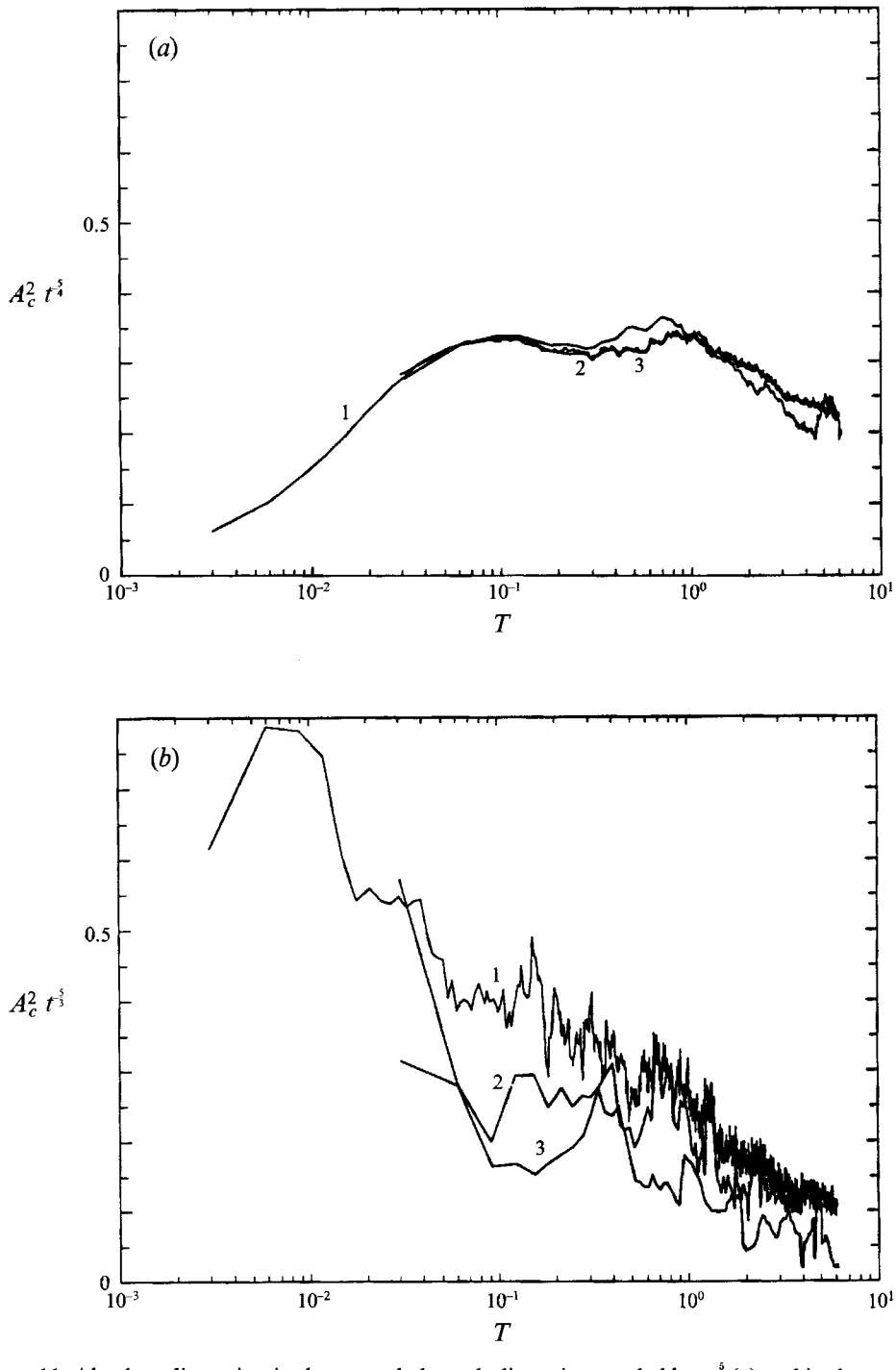

FIGURE 11. Absolute dispersion in the strongly hyperbolic regions scaled by $t^{-\frac{5}{4}}$ (*a*) and in the strongly elliptic regions scaled by $t^{-\frac{5}{3}}$ (*b*). Curves labelled 1 correspond to a conditional average (A II) with $m = 1$, curves labelled 2 correspond to (A II) with $m = 10$ *or* $m = 8$, curves labelled 3 correspond to (A I) with $m = 10$ or $m = 8$. Experiment R128F10.

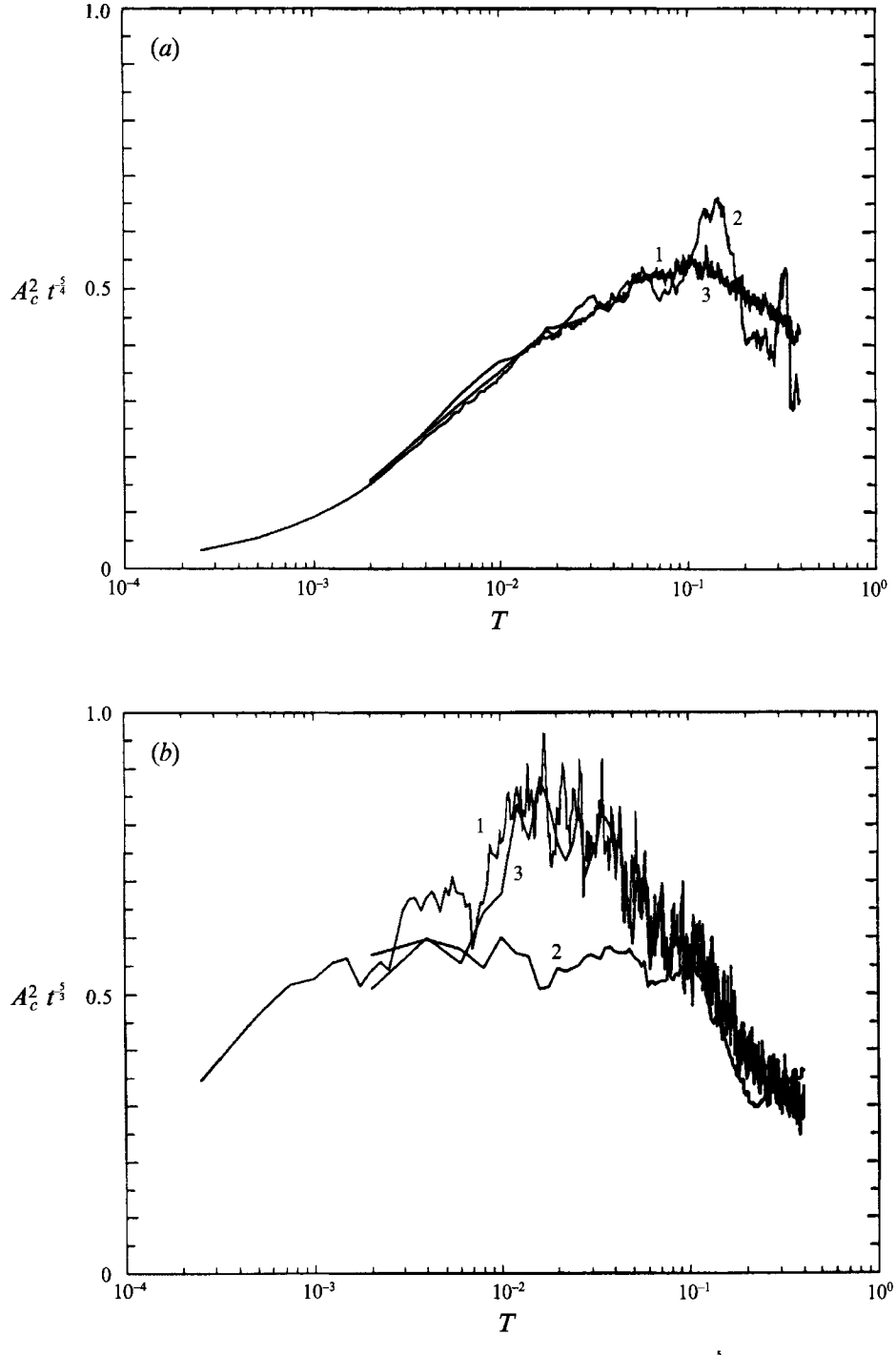

FIGURE 12. Absolute dispersion in the strongly hyperbolic regions scaled by $t^{-\frac{5}{4}}$ (*a*) and in the strongly elliptic regions scaled by $t^{-\frac{5}{3}}$ (*b*). Curves labelled 1 correspond to a conditional average (A II) with $m = 1$, curves labelled 2 correspond to (A II) with $m = 10$ or $m = 8$, curves labelled 3 correspond to (A I) with $m = 10$ or $m = 8$. Experiment R512F40.

with three different time averages: (A I) with $m = 10$ for R128F10 and $m = 8$ for R512F40; (A II) with $m = 1$ and $m = 10$ for R128F10; and $m = 1$ and $m = 8$ for R512F40.

Figure 10(a, b) shows the results of the analysis. In each part we have superposed the curves corresponding to the different types of conditional averages for the two experiments. Curves A refer to $\overline{Q^*} > 0.6$ and curves B to $\overline{Q^*} < -0.9$. Curves labelled 1 correspond to (A II) with $m = 1$, curves labelled 2 correspond to (A II) with $m = 10$ or $m = 8$, curves labelled 3 correspond to (A I) with $m = 10$ or $m = 8$. The dispersion in strongly hyperbolic regions is very weakly sensitive to the different types of conditional averages. For both R128F10 and R512F40, the $t^{\frac{5}{4}}$ law is clearly confirmed for hyperbolic regions. The effect of choosing different types of conditional averages is more important for dispersion in elliptic regions. In general, in these regions the duration of the small-time ballistic regime is clearly shortened, as a result of which the intermediate time dispersion law is steeper but less effective. At intermediate times, the dispersion in strongly elliptic regions (curves B 1, B 2 and B 3) seems to be dominated by an anomalous dispersion law $A_c^2 \propto t^{\frac{5}{3}}$. Note that a $t^{\frac{5}{3}}$ law would be consistent with the observed single-particle dispersion of freely drifting buoys in mesoscale ocean flows (see e.g. Provenzale *et al.* 1991).

To better characterize the correct slope of the anomalous dispersion laws, in figures 11(a, b) and 12(a, b) we show the absolute dispersion curves displayed in figure 10(a, b) scaled respectively by $t^{-\frac{5}{4}}$ and $t^{-\frac{5}{3}}$. A clear plateau in $A_c^2 t^{-\frac{5}{4}}$ emerges for the R128F10 experiment, while it is less prominent for the R512F40 experiment. Conversely, a plateau in $A_c^2 t^{-\frac{5}{3}}$ is clearly visible for R512F40, while it is almost absent for R12F10. The differences between the two experiments are most probably due to a different extension of the hyperbolic and elliptic regions in the R128F10 and R512F40 fields induced by the different forcing scale. In general, the above results indicate that the $t^{\frac{5}{4}}$ law is quite robust and it is observed independently of the amplitude of $\overline{Q^*}$. By contrast, the appearance of a $t^{\frac{5}{3}}$ law strongly depends on the value of the threshold $\overline{Q^*}$ used to build the conditional averages; this law is observed only for strongly elliptic regions and it is less robust.

5. Summary and conclusions

In this work we have studied the dynamics and the dispersion properties of passively advected neutral particles in two-dimensional turbulence. The results of the numerical simulations discussed here indicate that the single-particle dispersion properties are clearly affected by the characteristic topology of two-dimensional turbulence, as parametrized by the Weiss criterion (Weiss 1981) which provides a segmentation of the turbulent field into elliptic and hyperbolic regions. In fact, we have shown that the dispersion properties in hyperbolic and elliptic regions of the flow, characterized respectively by $Q > 0$ and $Q < 0$, are quite different. For example, the duration of the small-time ballistic regime, $A^2 \propto t^2$, is definitely shorter in elliptic regions than in hyperbolic ones.

The careful study of single-particle dispersion and the use of appropriate conditional averages on the set of advected particles has led to the discovery of two intermediate regimes of anomalous diffusion. At intermediate times, absolute dispersion in hyperbolic regions is characterized by a scaling law $A^2 \propto t^{\frac{5}{4}}$, while dispersion in highly elliptic regions is characterized by an intermediate dispersion law $A^2 \propto t^{\frac{5}{3}}$. Although the steepness of the power law in elliptic regions is larger than in hyperbolic domains, the absolute dispersion A^2 is in general less effective in elliptic regions owing to the more

limited duration of the small-time ballistic regime in these domains (i.e. in general $A^2_{ell} < A^2_{hyp}$). The two intermediate dispersion laws have, however, a very different robustness. In fact, the presence of the t^3 law is independent of the precise value of the threshold $\overline{Q^*}$, the requirement $\overline{Q^*} > 0$ being sufficient. In addition, this law is found for the ensemble of hyperbolic regions, independent of their energy and of the fact that they may be circulation cells or hyperbolic patches in the background turbulence. By contrast, the $t^{\frac{5}{3}}$ law is much less robust; in fact, this is clearly observed only for strongly elliptic regions where $\overline{Q^*} \approx -1$.

When global (unconditioned) averages on particle dispersions are considered, the intermediate anomalous dispersion regime associated with the action of hyperbolic domains is still often observed. This is because the different domains of the turbulent field are not equally sampled by the advected particles. In fact, the analysis of the particle concentration in the different topological domains indicates that neutral particles tend to leave elliptic regions (such as the vortex cores) and to concentrate in hyperbolic regions where deformation dominates rotation. In particular, the particle distribution displays a marked tendency to concentrate in the proximity of the isolines $\omega = 0$. As a consequence of this, the action of hyperbolic regions is predominant on the particle dispersion processes; the intermediate dispersion law typical of these domains is robustly observed on the global properties of absolute dispersion. This confirms that Lagrangian tracking of neutral particles does not provide a good measure of the elliptic regions of the flow.

Interestingly, recent measurements of drifter dispersion in turbulent flows have indicated the presence of an intermediate scaling law $A^2 \propto t^{\frac{5}{3}}$. If this result were interpreted in the framework of the two-dimensional turbulent dynamics considered here, then it would indicate that the drifters preferentially sample the elliptic regions of the flow. However, we have shown here that neutral particles tend to concentrate in hyperbolic domains. A possible explanation of this apparent discrepancy may rely upon the fact that drifters are not perfect (neutral) Lagrangian tracers, they may consequently behave quite differently from the neutral particles considered here. A study of the dispersion properties of non-perfect Lagrangian tracers (such as heavy and light impurities, see e.g. Crisanti *et al.* 1992) will be addressed in a future study.

REFERENCES

Babiano, A., Basdevant, C., Legras, B. & Sadourny, R. 1987*a* Vorticity and passive-scalar dynamics in two-dimensional turbulence. *J. Fluid Mech.* **183**, 379–397.

Babiano, A., Basdevant, C., Le Roy, P. & Sadourny, R. 1987*b* Single-particle dispersion, Lagrangian structures function and Lagrangian energy spectrum in two-dimensional incompressible turbulence. *J. Mar. Res.* **45**, 107–131.

Babiano, A., Basdevant, C., Le Roy, P. & Sadourny, R. 1990 Relative dispersion in two-dimensional turbulence. *J. Fluid Mech.* **214**, 535–557.

Babiano, A., Boffetta, G., Provenzale, A. & Vulpiani, A. 1993 Chaotic advection in point vortex models and 2-D turbulence. *Phys. Fluids* A (submitted).

Babiano, A. & Zouari, N. 1993 Eulerian and Lagrangian dispersion capacities in two-dimensional turbulence. *J. Fluid Mech.* (submitted)

Bartello, P. & Holloway, G. 1991 Passive scalar transport in β-plane turbulence. *J. Fluid Mech.* **223**, 521–536.

Basdevant, C., Legras, B., Sadourny, R. & Béland, M. 1981 A study of barotropic model flows: Intermittency waves and predictability. *J. Atmos. Sci.* **38**, 2305–2326.

Benzi, R., Paladin, G., Patarnello, S., Santangelo, P. & Vulpiani, A. 1986 Intermittency and coherent structures in two-dimensional turbulence. *J. Phys.* A: *Math. Gen.* **19**, 3771–3784.

BENZI, R., PATARNELLO, S. & SANTANGELO, P. 1987 On the statistical properties of two-dimensional decaying turbulence. *Europhys. Lett.* **3**, 811–818.

BENZI, R., PATARNELLO, S. & SANTANGELO, P. 1988 Self-similar coherent structures in two-dimensional deaying turbulence. *J. Phys.* A: *Math. Gen.* **21**, 1221–1237.

BRACHET, M., MENEGUZZI, M., POLITANO, H. & SULEM, P. 1988 The dynamics of freely decaying two-dimensional turbulence. *J. Fluid Mech.* **194**, 333–349.

CRISANTI, A., FALCIONI, M., PROVENZALE, A., TANGA, P. & VULPIANI, A. 1992 Dynamics of passively advected impurities in simple two-dimensional flow models. *Phys. Fluids* A **4**, 1805–1820.

HAIDVOGEL, D. B. 1982 On the feasibility of particle tracking in Eulerian ocean models. *Ocean Model.* **45**, 4–9.

LEGRAS, B., SANTANGELO, P. & BENZI, R. 1988 High-resolution numerical experiments for forced two-dimensional turbulence. *Europhys. Lett.* **5**, 37–42.

MCWILLIAMS, J. C. 1984 The emergence of isolated coherent vortices in turbulent flow. *J. Fluid Mech.* **146**, 21–43.

MCWILLIAMS, J. C. 1990 The vortices of two-dimensional turbulence. *J. Fluid Mech.* **219**, 361–385.

OHKITANI, K. 1991 Wave number space dynamics of enstrophy cascade in a forced two-dimensional turbulence. *Phys. Fluids* A **3**, 1598–1611.

OSBORNE, A. R., KIRWAN, A. D., PROVENZALE, A. & BERGAMASCO, L. 1989 Fractal drifter trajectories in the Kuroshio extension. *Tellus* **41A**, 416–435.

PROVENZALE, A., OSBORNE, A. R., KIRWAN, A. D. & BERGAMASCO, L. 1991 The study of fluid parcel trajectories in large-scale ocean flows. In *Nonlinear Topics in Ocean Physics* (ed. A. R. Osborne), pp. 367–401. Elsevier.

SANDERSON, B. G. & BOOTH, D. A. 1991 The fractal dimension of drifter trajectories and estimates of horizontal eddy-diffusivity. *Tellus* **43A**, 334–349.

SANDERSON, B. G., GOULDING, A. & OKUBO, A. 1990 The fractal dimension of relative Lagrangian motion. *Tellus* **42A**, 550–556.

TAYLOR, G. I. 1921 Diffusion by continuous movement. *Proc. Lond. Math. Soc.* **20**, 196–212.

WEISS, J. 1981 The dynamics of enstrophy transfer in two-dimensional hydrodynamics. *LJI-TN-121ss*, La Jolla Inst., La Jolla. CA.

ZOUARI, N. & BABIANO, A. 1990 Experiences numériques lagrangiennes à partir de modèles eulériens. *Atmos. Ocean* **28**, 345–364.

ZOUARI, N. 1991 Dispersion lagrangienne en turbulence bidimensionelle. D. Thesis, Université de Paris 6.